Turkish Journal of Electrical Engineering & Computer Sciences

http://journals.tubitak.gov.tr/elektrik/

Research Article

Turk J Elec Eng & Comp Sci
(2018) 26: 378 – 392
© TÜBİTAK
doi:10.3906/elk-1705-167

Neural network-based adaptive tracking control for a nonholonomic wheeled mobile robot with unknown wheel slips, model uncertainties, and unknown bounded disturbances

Tinh NGUYEN[1,*], **Linh LE**[2]
[1]Department of Automation Technology, Institute of Information Technology, Vietnam Academy of Science and Technology, Hanoi, Vietnam
[2]University of Information and Communication Technology, Thai Nguyen University, Thai Nguyen, Vietnam

Received: 15.05.2017 • **Accepted/Published Online:** 22.09.2017 • **Final Version:** 26.01.2018

Abstract: In this paper, an adaptive tracking controller based on a three-layer neural network (NN) with an online weight tuning algorithm is proposed for a nonholonomic wheeled mobile robot in the presence of unknown wheel slips, model uncertainties, and unknown bounded disturbances. The online weight tuning algorithm is modified from the backpropagation with an e-modification term required to assure that the NN weights are bounded. Preliminary neural network offline training is not essential for the weights. Thanks to this proposed controller, the desired tracking performance is achieved where position tracking errors converge to an arbitrarily small neighborhood of the origin regardless of their initial values. According to Lyapunov theory and LaSalle extension, the stability of the whole closed-loop system is ensured to obtain the desired tracking performance. Computer simulations are implemented to certify the validity of the proposed controller.

Key words: Desired tracking performance, online weight tuning algorithm, position tracking errors, uniformly ultimately bounded, unknown wheel slip

1. Introduction

In recent years, due to the fact that wheeled mobile robots (WMRs) are widely applied and increasingly popular, a lot of the effort of researchers in the world has been spent to solve the tracking control problems of WMRs by using various control techniques such as sliding mode control [1], adaptive control [2], and backstepping control [3,4]. All these works have been performed with an assumption that WMRs move on the floor without wheel slips.

However, unfortunately, in many practical applications, the assumption of "pure rolling without slip" is often violated. In other words, wheel slips exist. Wheel slip depends on many various factors, such as an unknown centrifugal force possibly acting on the WMR when it moves in a circular path, an external force acting on the WMR, or a weak frictional force between the slippery floor and the wheels. Wheel slips have made the tracking performance of WMRs considerably worse. Consequently, if one wishes a tracking control problem to be solved effectively in such a context, then a tracking controller, which is able to achieve a desired tracking performance in the presence of wheel slips, has to be considered.

Particularly, with the purpose of compensating the undesired effect of wheel slips, an adaptive tracking

[*] Correspondence: nvtinh@ioit.ac.vn

controller was derived through a radial basis function neural network [5]. However, this work only dealt with longitudinal slips of each driving wheel; lateral slip was not considered. Methods based on gyros and accelerometers to deal with wheel slips in real time were also described in [6,7]. The authors of [8] proposed a feedback linearization controller for tracking a desired trajectory of a WMR in the presence of longitudinal and lateral slip at each driving wheel under ideal conditions where model uncertainties did not exist, such as unstructured unmodeled dynamic components and unknown bounded disturbances such as unknown bounded external forces, and the values of the accelerations and velocities of the wheel slip could be measured exactly. Nonetheless, it is impractical to achieve a good performance by using this feedback linearization controller in real applications as the ideal condition is unrealistic.

To summarize, most of these works were based on an assumption that the measurements of the accelerations and velocities of the wheel slips were available for analyzing and designing slip-compensation controllers. The disadvantage of this assumption is the requirement of extra sensors to measure the wheel slips, such as a global position system (GPS), a gyroscope, and an accelerometer, which are expensive and complex.

These results have motivated us to design a novel neural network-based adaptive tracking controller for a WMR with unknown wheel slips such that the WMR tracks a desired trajectory with the desired tracking performance. Furthermore, measurements of the wheel slips are no longer essential.

2. Materials and methods

2.1. The kinematics of a nonholonomic WMR in the presence of wheel slips

Let us consider a nonholonomic WMR, which comprises two driving wheels and a caster wheel, as in Figure 1. Namely, G with coordinates (x_G, y_G) is the center of mass of the platform of the WMR. M with coordinates (x_M, y_M) is the midpoint of the wheel shaft. F_1 and F_2 are the total longitudinal friction forces at the right and left wheel, respectively. F_3 is the total lateral friction force along the wheel shaft. F_4 and ϖ are external force and moment acting on G, respectively. r is the radius of each driving wheel. b is the haft of the wheel shaft. θ is the orientation of the WMR.

In the absence of wheel slip, the linear and angular velocities of the WMR, computed at M, are represented

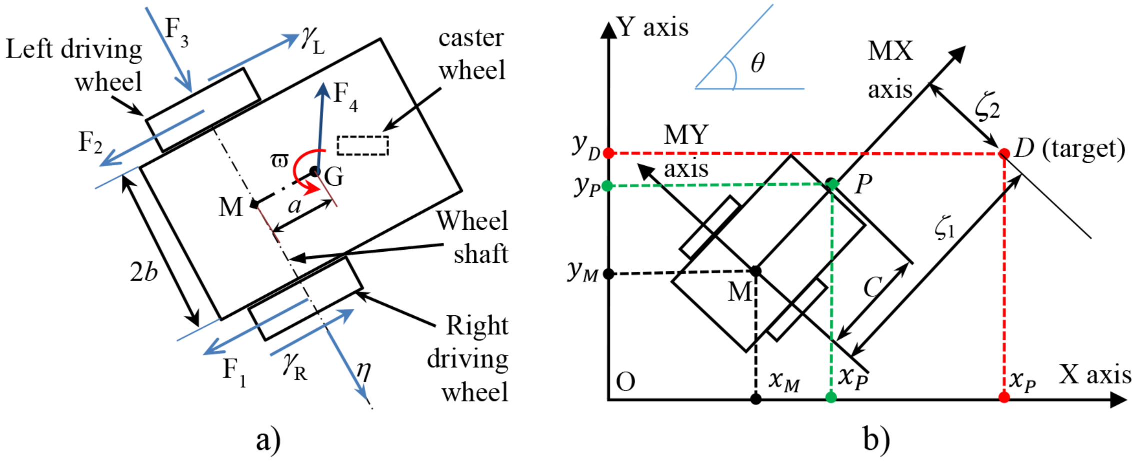

Figure 1. a) The nonholonomic WMR subject to wheel slip. b) The coordinates of the target are represented in the body coordinate system M-XY.

respectively as follows:

$$\Theta = r\left(\dot{\phi}_R + \dot{\phi}_L\right)2,\ \mu = r(\dot{\phi}_R - \dot{\phi}_L)/(2b) \tag{1}$$

where $\dot{\phi}_R$ and $\dot{\phi}_L$ are the angular velocities of the right and left wheel about the wheel shaft, respectively.

Hence, the kinematics of the WMR is written as follows:

$$\begin{cases} \dot{x}_M = \Theta\cos\theta \\ \dot{y}_M = \Theta\sin\theta \\ \dot{\theta} = \mu \end{cases} \tag{2}$$

Alternatively, when the WMR moves in the presence of slips between the wheels and the floor, Eqs. (1) and (2) are no longer true. Now let γ_R and γ_L denote the coordinates of the longitudinal slip of the right and left wheels, respectively, and η denote the coordinate of the lateral slip along the wheel shaft (see Figure 1a). In this case, the actual linear velocity of the WMR along the longitudinal direction is as follows:

$$\Omega = \frac{r(\dot{\phi}_R + \dot{\phi}_L)}{2} + \frac{\dot{\gamma}_R + \dot{\gamma}_L}{2} = \Theta + \dot{\chi},\ \text{with}\ \chi = (\gamma_R + \gamma_L)/2 \tag{3}$$

The actual angular velocity of the WMR is computed as follows:

$$\omega = \frac{r(\dot{\phi}_R - \dot{\phi}_L)}{2b} + \frac{\dot{\gamma}_R - \dot{\gamma}_L}{2b} = \mu + \vartheta,\ \text{with}\ \vartheta = \frac{\dot{\gamma}_R - \dot{\gamma}_L}{2b} \tag{4}$$

Thus, the kinematic model of this WMR can be expressed as follows:

$$\begin{cases} \dot{x}_M = \Omega\cos\theta - \dot{\eta}\sin\theta \\ \dot{y}_M = \Omega\sin\theta + \dot{\eta}\cos\theta \\ \dot{\theta} = \omega \end{cases} \tag{5}$$

In this case, the perturbed nonholonomic constrains can be written as follows:

$$\begin{cases} \dot{\gamma}_R = -r\dot{\phi}_R + \dot{x}_M\cos\theta + \dot{y}_M\sin\theta + b\omega \\ \dot{\gamma}_L = -r\dot{\phi}_L + \dot{x}_M\cos\theta + \dot{y}_M\sin\theta - b\omega \\ \dot{\eta} = -\dot{x}_M\sin\theta + \dot{y}_M\cos\theta \end{cases}. \tag{6}$$

2.2. The dynamics of the nonholonomic WMR with wheel slips

Let $\mathbf{q} = [x_G,\ y_G,\ \theta,\ \eta,\ \gamma_R,\ \gamma_L,\ \phi_R,\ \phi_L]^{\mathbf{T}}$ be a generalized Lagrange coordinate vector. The perturbed nonholonomic constraints of Eq. (6) can be rewritten as follows:

$$\mathbf{A}(\mathbf{q})\,\dot{\mathbf{q}} = \mathbf{0}\ \text{where}\ \mathbf{A}(\mathbf{q}) = \begin{bmatrix} \cos\theta & \sin\theta & b & 0 & -1 & 0 & -r & 0 \\ \cos\theta & \sin\theta & -b & 0 & 0 & -1 & 0 & -r \\ -\sin\theta & \cos\theta & -a & -1 & 0 & 0 & 0 & 0 \end{bmatrix}, \tag{7}$$

where a is the distance between M and G.

The dynamic equation of the whole system can be represented by

$$\overline{\mathbf{M}}\ddot{\mathbf{q}}+\bar{\boldsymbol{\tau}}_{\mathbf{d}}=\mathbf{N}\boldsymbol{\tau}+\mathbf{A}^{\mathbf{T}}(\mathbf{q})\boldsymbol{\lambda}, \tag{8}$$

where $\boldsymbol{\lambda}=[\lambda_1,\lambda_2,\lambda_3]^T$ is the vector of Lagrange multipliers to be considered as unknown nonholonomic constraint forces. $\boldsymbol{\tau}=[\tau_R,\tau_L]^T$ is the input vector with τ_R and τ_L being the torques at the right and left wheel about the wheel shaft, respectively. $\bar{\boldsymbol{\tau}}_{\mathbf{d}}$ is a vector illustrating model uncertainties such as the unstructured unmodeled dynamic components and unknown bounded disturbances such as the unknown external forces as F_1, F_2, F_3, F_4, ϖ (see Figure 1a). $\mathbf{N}=\begin{bmatrix}0&0&0&0&0&0&1&0\\0&0&0&0&0&0&0&1\end{bmatrix}^T$ is the input transformation matrix.

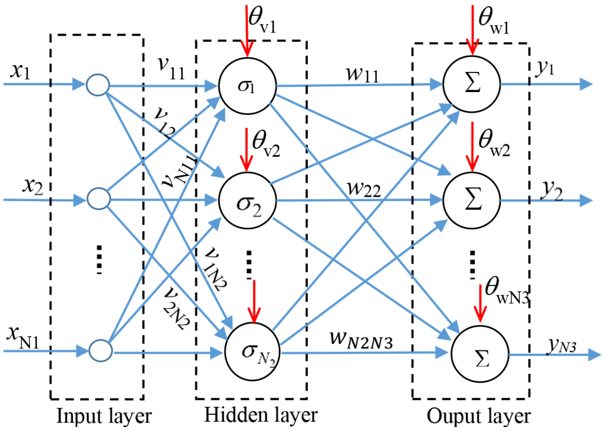

Figure 2. Structure of a three-layer neural network.

In contrast, it is easy to achieve the following equation:

$$\dot{\mathbf{q}}=\mathbf{S}_1\left(\mathbf{q}\right)\mathbf{v}+\mathbf{S}_2\left(\mathbf{q}\right)\dot{\boldsymbol{\gamma}}+\mathbf{S}_3(\mathbf{q})\dot{\eta} \tag{9}$$

where $\mathbf{v}=\left[\dot{\phi}_R,\dot{\phi}_L\right]^T$, $\boldsymbol{\gamma}=[\gamma_R,\gamma_L]^T$,

$$\mathbf{S}_1\left(\mathbf{q}\right)=\begin{bmatrix}\left(\frac{r}{2}\cos\theta-\frac{ar}{2b}\sin\theta\right)&\frac{r}{2b}&0&0&0&1&0\\\left(\frac{r}{2}\sin\theta+\frac{ar}{2b}\cos\theta\right)&-\frac{r}{2b}&0&0&0&0&1\end{bmatrix}^T,$$

$$\mathbf{S}_2\left(\mathbf{q}\right)=\begin{bmatrix}\left(\frac{1}{2}\cos\theta-\frac{a}{2b}\sin\theta\right)&\frac{1}{2b}&0&1&0&0&0\\\left(\frac{1}{2}\sin\theta+\frac{a}{2b}\cos\theta\right)&-\frac{1}{2b}&0&0&1&0&0\end{bmatrix}^T,$$

$$\mathbf{S}_3(\mathbf{q})\;=\;[-\sin\theta\quad\cos\theta\;\;0\;\;1\;\;0\;\;0\;\;0\;\;0]^T$$

Next, taking the time derivative of Eq. (9), we obtain:

$$\ddot{\mathbf{q}}=\dot{\mathbf{S}}_1\left(\mathbf{q}\right)\mathbf{v}+\mathbf{S}_1\left(\mathbf{q}\right)\dot{\mathbf{v}}+\dot{\mathbf{S}}_2\left(\mathbf{q}\right)\dot{\boldsymbol{\gamma}}+\mathbf{S}_2\left(\mathbf{q}\right)\ddot{\boldsymbol{\gamma}}+\dot{\mathbf{S}}_3(\mathbf{q})\dot{\eta}+\mathbf{S}_3(\mathbf{q})\ddot{\eta} \tag{10}$$

It is useful to show that $\mathbf{S}_1^T(\mathbf{q})\,\mathbf{A}^T(\mathbf{q}) = \mathbf{0}_{2\times 3}$, $\mathbf{S}_1^T(\mathbf{q})\,\mathbf{N} = \mathbf{I}_{2\times 2}$, where $\mathbf{I}_{2\times 2}$ is a unit 2×2 matrix and $\mathbf{0}_{2\times 3}$ is an $i \times j$ zero matrix. Substituting Eq. (10) into Eq. (8), and then premultiplying both sides of the new equation by $\mathbf{S}_1^T(\mathbf{q})$, we get:

$$\mathbf{M}\dot{\mathbf{v}} + \mathbf{B}\mathbf{v} + \mathbf{Q}\ddot{\boldsymbol{\gamma}} + \mathbf{C}\dot{\eta} + \mathbf{G}\ddot{\eta} + \boldsymbol{\tau}_{\mathbf{d}} = \boldsymbol{\tau}, \tag{11}$$

where

$$\boldsymbol{\tau}_{\mathbf{d}} = \mathbf{S}_1^T(\mathbf{q})\,\overline{\boldsymbol{\tau}}_{\mathbf{d}},\ \mathbf{M} = \mathbf{S}_1^T(\mathbf{q})\,\overline{\mathbf{M}}\mathbf{S}_1(\mathbf{q}) = \begin{bmatrix} m_{11} & m_{12} \\ m_{12} & m_{11} \end{bmatrix}$$

$$\mathbf{Q} = \mathbf{S}_1^T(\mathbf{q})\,\overline{\mathbf{M}}\mathbf{S}_2(\mathbf{q}) = \begin{bmatrix} Q_1 & Q_2 \\ Q_2 & Q_1 \end{bmatrix},\ \mathbf{C} = \mathbf{S}_1^T(\mathbf{q})\,\overline{\mathbf{M}}\dot{\mathbf{S}}_3(\mathbf{q}) = m_G\frac{r}{2}\omega\begin{bmatrix} 1 \\ 1 \end{bmatrix},$$

$$\mathbf{G} = \mathbf{S}_1^T(\mathbf{q})\,\overline{\mathbf{M}}\mathbf{S}_3(\mathbf{q}) = m_G\frac{ar}{2b}\begin{bmatrix} 1 \\ -1 \end{bmatrix},\ \mathbf{B} = \mathbf{S}_1^T(\mathbf{q})\,\overline{\mathbf{M}}\dot{\mathbf{S}}_1(\mathbf{q}) = m_G\frac{ar^2}{2b}\omega\begin{bmatrix} 0 & 1 \\ -1 & 0 \end{bmatrix},$$

with

$$m_{11} = m_G\left(\frac{r^2}{4} + \frac{a^2r^2}{4b^2}\right) + \frac{r^2}{4b^2}\left(I_G + 2I_D\right) + 2m_w r^2 + I_W,$$

$$m_{12} = m_G\left(\frac{r^2}{4} - \frac{a^2r^2}{4b^2}\right) - \frac{r^2}{4b^2}\left(I_G + 2I_D\right), Q_{1,2} = m_G\frac{r}{4}\left(1 \pm \frac{a^2}{b^2}\right) \pm \frac{r}{4b}\left(I_G + 2I_D\right).$$

The parameters of the WMR in the matrices revealed above are described in the Table.

Table. The parameters of the WMR.

Symbol	Quantity	Value
m_G	The mass of the platform of the WMR	10 (kg)
I_G	The inertial moment of the platform about the vertical axis through point G (Figure 1a)	4 (kgm^2)
a	The distance between G and M (Figure 1a)	0.2 (m)
C	The distance between P and M (Figure 1b)	0.5 (m)
m_W	The mass of each driving wheel	2 (kg)
I_W	The inertial moment of each wheel about its rotational axis	0.1 (kgm^2)
I_D	The inertial moment of each wheel about its diameter axis	0.05 (kgm^2)
b	The half-distance between the two driving wheels	0.3 (m)
r	The radius of each wheel	0.15 (m)

2.3. Problem statement

Let D with coordinates (x_D, y_D) be a target that is moving in a known desired trajectory (see Figure 1b). The requirement of the tracking control problem is to control the WMR so that P with coordinates (x_P, y_P) has to track D with position tracking errors being uniformly ultimately bounded.

Remark 1 *Let (x_P, y_P, θ) be the actual posture of the WMR and $(x_{Pd}, y_{Pd}, \theta_d)$ be the desired one of the WMR. The presence of both the longitudinal and lateral slip makes it impossible to control the WMR so that the actual posture tracks the desired one with an arbitrarily good tracking performance. By contrast, it is fully possible in order to control the WMR with the aim of making the actual position (x_P, y_P) track the desired one (x_{Pd}, y_{Pd}) with an arbitrarily good tracking performance (see Definition 1 and Definition 2 in [9]).*

2.4. Representing the vector of filtered tracking errors

Let O-XY be the global coordinate system and let M-XY be the body coordinate system that is attached to the platform of the WMR (see Figure 1b). The coordinate vector of target D is represented in M-XY as follows:

$$\boldsymbol{\zeta} = \begin{bmatrix} \zeta_1 \\ \zeta_2 \end{bmatrix} = \begin{bmatrix} \cos\theta & \sin\theta \\ -\sin\theta & \cos\theta \end{bmatrix} \begin{bmatrix} x_D - x_M \\ y_D - y_M \end{bmatrix}. \tag{12}$$

Taking the second-order derivative with respect to time of Eq. (12) yields

$$\ddot{\boldsymbol{\zeta}} = \mathbf{h}\dot{\mathbf{v}} + \boldsymbol{\Psi}_1 + \boldsymbol{\Psi}_2, \tag{13}$$

where

$$\boldsymbol{\Psi}_1 = \begin{bmatrix} \dot\zeta_2\mu + \ddot x_D\cos\theta + \ddot y_D\sin\theta - \dot x_D\mu\sin\theta + \dot y_D\mu\cos\theta \\ -\dot\zeta_1\mu - \ddot x_D\sin\theta + \ddot y_D\cos\theta - \dot x_D\mu\cos\theta - \dot y_D\mu\sin\theta \end{bmatrix},$$

$$\boldsymbol{\Psi}_2 = \begin{bmatrix} -\ddot\chi - \zeta_2\dot\vartheta - \dot\zeta_2\vartheta - \dot x_D\vartheta\sin\theta + \dot y_D\vartheta\cos\theta \\ -\ddot\eta - \zeta_1\dot\vartheta - \dot\zeta_1\vartheta - \dot x_D\vartheta\cos\theta - \dot y_D\vartheta\sin\theta \end{bmatrix},$$

and

$$\mathbf{h} = \begin{bmatrix} \left(\frac{\zeta_2}{b} - 1\right)\frac{r}{2} & -\left(\frac{\zeta_2}{b} + 1\right)\frac{r}{2} \\ -\frac{\zeta_1}{b}\frac{r}{2} & \frac{\zeta_1}{b}\frac{r}{2} \end{bmatrix}, \text{ with } \mu = \frac{r\left(\dot\phi_R - \dot\phi_L\right)}{2b}, \vartheta = \frac{\dot\gamma_R - \dot\gamma_L}{2b}, \chi = \frac{\gamma_R + \gamma_L}{2}.$$

Remark 2 *Owing to* $\det(\mathbf{h}) = -\zeta_1 r^2/(2b)$, *if* $\zeta_1 \neq 0$, *then* $\mathbf{h}$ *is an invertible matrix. Let us define the position tracking error vector as* $\mathbf{e} = [e_1, e_2]^T = \boldsymbol{\zeta} - \boldsymbol{\zeta}_\mathbf{d}$ *where* $\boldsymbol{\zeta}_\mathbf{d}$ *is the desired coordinate vector of the target in M-XY. From the requirement of the position tracking control problem mentioned above and Figure 1b, one can easily show* $\boldsymbol{\zeta}_\mathbf{d} = [C, 0]^T$, *with* C *showing the distance between P and M.*

The filtered tracking error vector is defined as follows:

$$\boldsymbol{\varphi} = \dot{\mathbf{e}} + \boldsymbol{\Lambda}\mathbf{e} \tag{14}$$

where Λ is a 2 × 2 diagonal, constant, positive definite matrix and is chosen arbitrarily.

2.5. Three-layer neural network (NN)

One cannot deny that artificial neural networks have the ability of approximating nonlinear and sufficiently smooth functions with arbitrary accuracy. In this subsection, a three-layer NN is introduced briefly [3]. As illustrated in Figure 2, the output of the NN can be computed as $\mathbf{y}(\mathbf{x}, \mathbf{W}, \mathbf{V}) = [y_1, \ldots, y_{N_3}]^\mathbf{T} = \mathbf{W}^\mathbf{T}\boldsymbol{\sigma}\left(\mathbf{V}^\mathbf{T}\mathbf{x}\right)$ where $\mathbf{x} = [1, x_1, \ldots, x_{N_1}]^\mathbf{T}$ is the input vector, and $\mathbf{W} = [\mathbf{w_{ij}}]$ and $\mathbf{V} = [v_\mathbf{ij}]$ are the NN weight matrices. $\boldsymbol{\sigma}(\mathbf{z}) = [1, \sigma(z_1), \sigma(z_2), \ldots]^\mathbf{T}$ with $\mathbf{z} = [z_1, z_2, \ldots]^\mathbf{T}$. Next, $\sigma(\bullet)$ is the activation function of the NN. In this paper, the activation function is chosen to be the sigmoid kind as $\sigma(z) = 1/(1 + \exp(-z))$.

To be specific, one can write the following:

$$y_i = \sum_{j=1}^{N_2}\left[w_{ij}\sigma\left(\theta_{vj} + \sum_{k=1}^{N_1} v_{jk}x_k\right)\right] + \theta_{wi}, i = 1, 2, 3, \ldots, N_3, \tag{15}$$

where N_1, N_2, and N_3 are the number of neurons of the input layer, hidden layer, and output layer, respectively. Next, v_{ij} and w_{ij} are flexible weights that interconnect the input with the hidden layer and the hidden with the output layer, respectively. θ_{wi} and θ_{vj} are the threshold offsets of the output and hidden layer, respectively.

It is interesting that inserting 1 as the first component of $\mathbf{x}$ allows one to include the threshold vector $[\theta_{v1},\theta_{v2},\ldots,\theta_{vN_1}]^{\mathbf{T}}$ as the first row of $\mathbf{V}$. Likewise, $\boldsymbol{\sigma}(\mathbf{z})$ containing 1 as the first term permits the threshold vector $[\theta_{w1},\theta_{w2},\ldots,\theta_{wN_3}]^{\mathbf{T}}$ to be the first row of $\mathbf{W}$. For this reason, any tuning of $\mathbf{W}$ and $\mathbf{V}$ is composed of tuning of the weights w_{ij}, $v_{\mathbf{ij}}$ as well as the thresholds θ_{wi}, θ_{vj}.

Let $\mathbf{f}(\mathbf{x}) : \mathbf{R}^{\mathbf{N_1}} \to \mathbf{R}^{\mathbf{N_3}}$ be a continuous function. There exist ideal weight matrices $\mathbf{W}$ and $\mathbf{V}$ such that:

$$\mathbf{f}(\mathbf{x}) = \mathbf{W}^{\mathbf{T}}\boldsymbol{\sigma}\left(\mathbf{V}^{\mathbf{T}}\mathbf{x}\right) + \boldsymbol{\varepsilon}, \tag{16}$$

where $\boldsymbol{\varepsilon}$ is the vector of reconstruction errors.

Assumption 1 *$\boldsymbol{\varepsilon}$ is bounded. Namely, $\|\boldsymbol{\varepsilon}\| \leq \mathbf{b}_{\varepsilon}$ with $\mathbf{b}_{\varepsilon}$ being an upper bound of $\boldsymbol{\varepsilon}$. Let $\widehat{\mathbf{f}}\left(\mathbf{x},\widehat{\mathbf{W}},\widehat{\mathbf{V}}\right) = \widehat{\mathbf{y}}\left(\mathbf{x},\widehat{\mathbf{W}},\widehat{\mathbf{V}}\right) = \widehat{\mathbf{W}}\boldsymbol{\sigma}\left(\widehat{\mathbf{V}}^{\mathbf{T}}\mathbf{x}\right)$ denote an estimation of $\mathbf{f}(\mathbf{x})$, where $\widehat{\mathbf{W}}$ and $\widehat{\mathbf{V}}$ are estimation matrices of $\mathbf{W}$ and $\mathbf{V}$, respectively, and they are provided by an online weight tuning algorithm to be revealed subsequently.*

For convenience, let us denote $\boldsymbol{\sigma} = \boldsymbol{\sigma}\left(\mathbf{V}^{\mathbf{T}}\mathbf{x}\right)$, $\widehat{\boldsymbol{\sigma}} = \widehat{\boldsymbol{\sigma}}\left(\widehat{\mathbf{V}}^{\mathbf{T}}\mathbf{x}\right)$. The function approximation error vector is defined as follows:

$$\widetilde{\mathbf{f}} = \mathbf{f}(\mathbf{x}) - \widehat{\mathbf{f}}\left(\mathbf{x},\widehat{\mathbf{W}},\widehat{\mathbf{V}}\right) = \mathbf{W}^{T}\boldsymbol{\sigma} + \boldsymbol{\varepsilon} - \widehat{\mathbf{W}}^{T}\widehat{\boldsymbol{\sigma}}, \tag{17}$$

2.6. The structure of the controller

To begin with, let us propose the scheme of the whole closed-loop system as shown in Figure 3.

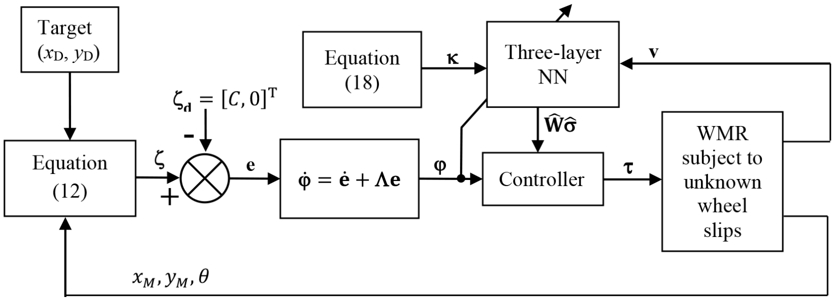

Figure 3. Scheme of control system.

Next, in Eq. (13), because of directly depending on the accelerations and velocities of the wheel slip, which are not measured in this work, $\Psi_{\mathbf{2}}$ is unknown. Therefore, let us define an auxiliary variable that can be measured easily as follows:

$$\boldsymbol{\kappa} = \mathbf{h}^{-1}(-\ddot{\boldsymbol{\zeta}}_{\mathbf{d}} + \boldsymbol{\Lambda}\dot{\mathbf{e}} + \boldsymbol{\Psi}_1) \tag{18}$$

Alternatively, one can rewrite Eq. (11) as follows:

$$\mathbf{M}\dot{\mathbf{v}} = \boldsymbol{\tau} - \mathbf{B}\mathbf{v} - \mathbf{d} - \boldsymbol{\tau}_{\mathbf{d}} \tag{19}$$

where $\mathbf{d} = \mathbf{Q}\ddot{\gamma} + \mathbf{C}\dot{\eta} + \mathbf{G}\ddot{\eta}$.

Adding $\mathbf{M}\boldsymbol{\kappa}$ to both sides of Eq. (19) and then combining the result with Eqs. (13), (14), and (18) leads to

$$\mathbf{M}\mathbf{h}^{-\mathbf{1}}\dot{\boldsymbol{\varphi}} = \boldsymbol{\tau} + \mathbf{M}\boldsymbol{\kappa} - \mathbf{B}\mathbf{v} - \mathbf{d} - \boldsymbol{\tau}_{\mathbf{d}} + \mathbf{M}\mathbf{h}^{-\mathbf{1}}\boldsymbol{\Psi}_{\mathbf{2}} \tag{20}$$

Conversely, it is difficult to specifically know parameters of the dynamics of this WMR such as mass or moments of inertia. Consequently, it is impossible to precisely illustrate all expressions including these quantities. Therefore, one can rewrite Eq. (20) as follows:

$$\widehat{\mathbf{M}}\mathbf{h}^{-\mathbf{1}}\dot{\boldsymbol{\varphi}} = \boldsymbol{\tau} - \widetilde{\mathbf{M}}\mathbf{h}^{-\mathbf{1}}\dot{\boldsymbol{\varphi}} + \mathbf{M}\boldsymbol{\kappa} - \mathbf{B}\mathbf{v} - \mathbf{d} + \mathbf{M}\mathbf{h}^{-\mathbf{1}}\boldsymbol{\Psi}_{\mathbf{2}} - \boldsymbol{\tau}_{\mathbf{d}} \tag{21}$$

where $\widetilde{\mathbf{M}} = \mathbf{M} - \widehat{\mathbf{M}}$ with $\widehat{\mathbf{M}}$ denoting an approximation of $\mathbf{M}$.

Remark 3 *It should be noted that both* $\mathbf{M}$ *and* $\widehat{\mathbf{M}}$ *are always symmetric, invertible, positive definite matrices.*

Remark 4 *In practice, the unknown wheel slips depend on the linear and angular velocities of the WMR [10].*

Multiplying both sides of Eq. (21) by $\mathbf{h}\widehat{\mathbf{M}}^{-\mathbf{1}}$ yields

$$\dot{\boldsymbol{\varphi}} = \mathbf{h}\widehat{\mathbf{M}}^{-\mathbf{1}}\boldsymbol{\tau} + \mathbf{f}(\mathbf{x}) + \boldsymbol{\Xi} \tag{22}$$

where $\mathbf{f}(\mathbf{x}) = \mathbf{h}\widehat{\mathbf{M}}^{-\mathbf{1}}[-\widetilde{\mathbf{M}}\mathbf{h}^{-\mathbf{1}}\dot{\boldsymbol{\varphi}} + \mathbf{M}\boldsymbol{\kappa} - \mathbf{B}\mathbf{v} - \mathbf{d} + \mathbf{M}\mathbf{h}^{-\mathbf{1}}\boldsymbol{\Psi}_{\mathbf{2}}]$. The vector $\mathbf{x}$ required so as to calculate $\mathbf{f}(\mathbf{x})$ can be determined by $\mathbf{x} = [1 \quad \mathbf{v}^T \quad \boldsymbol{\kappa}^T]^T$. Clearly, $\mathbf{x}$ can be measured easily. In addition, $\boldsymbol{\Xi} = -\mathbf{h}\widehat{\mathbf{M}}^{-\mathbf{1}}\boldsymbol{\tau}_{\mathbf{d}}$ expresses the model uncertainties as well as the unknown bounded disturbances.

Next, one can choose a torque-computing control law as follows:

$$\boldsymbol{\tau} = \widehat{\mathbf{M}}\mathbf{h}^{-\mathbf{1}}[-\mathbf{K}\boldsymbol{\varphi} - \widehat{\mathbf{f}}(\mathbf{x}, \widehat{\mathbf{W}}, \widehat{\mathbf{V}})] \tag{23}$$

where $\mathbf{K}$ is a 2 × 2 diagonal, constant, positive definite matrix and is chosen arbitrarily. $\widehat{\mathbf{f}}\left(\mathbf{x}, \widehat{\mathbf{W}}, \widehat{\mathbf{V}}\right)$ is the output of the NN in order to approximate $\mathbf{f}(\mathbf{x})$ as shown in Eq. (17).

Substituting Eq. (23) into Eq. (22) and then combining the result with Eq. (17) yields:

$$\dot{\boldsymbol{\varphi}} = -\mathbf{K}\boldsymbol{\varphi} + \mathbf{W}^{\mathbf{T}}\boldsymbol{\sigma} + \varepsilon - \widehat{\mathbf{W}}^{\mathbf{T}}\widehat{\boldsymbol{\sigma}} + \boldsymbol{\Xi} \tag{24}$$

On the other hand, one can write the Taylor series expansion around $\widehat{\mathbf{V}}$ for a known $\mathbf{x}$ as $\boldsymbol{\sigma} = \widehat{\boldsymbol{\sigma}} + \acute{\boldsymbol{\sigma}}\widetilde{\mathbf{V}}^{\mathbf{T}}\mathbf{x}$ $+\mathbf{O}(\widetilde{\mathbf{V}}^{\mathbf{T}}\mathbf{x})$ where $\acute{\boldsymbol{\sigma}} = \boldsymbol{\partial\sigma}(\mathbf{z})/\boldsymbol{\partial}\mathbf{Z}|_{\mathbf{z}=\mathbf{z}(\widehat{\mathbf{V}}\mathbf{x})}$, and $\mathbf{O}\left(\widetilde{\mathbf{V}}^{\mathbf{T}}\mathbf{x}\right)$ illustrates the second-order term and higher-order terms of the Taylor series, with $\widetilde{\mathbf{V}} = \mathbf{V} - \widehat{\mathbf{V}}$.

Let $\widetilde{\boldsymbol{\sigma}}$ be the error of the hidden layer as $\widetilde{\boldsymbol{\sigma}} = \boldsymbol{\sigma} - \widehat{\boldsymbol{\sigma}} = \acute{\boldsymbol{\sigma}}\widetilde{\mathbf{V}}^{\mathbf{T}}\mathbf{x} + \mathbf{O}(\widetilde{\mathbf{V}}^{\mathbf{T}}\mathbf{x})$.

Adding and subtracting $\mathbf{W}^{\mathbf{T}}\widehat{\boldsymbol{\sigma}}$ and $\widehat{\mathbf{W}}^{\mathbf{T}}\widetilde{\boldsymbol{\sigma}}$ results in:

$$\dot{\boldsymbol{\varphi}} = -\mathbf{K}\boldsymbol{\varphi} + \widetilde{\mathbf{W}}^{\mathbf{T}}\widetilde{\boldsymbol{\sigma}} + \widetilde{\mathbf{W}}^{\mathbf{T}}\widehat{\boldsymbol{\sigma}} + \widehat{\mathbf{W}}^{\mathbf{T}}\widetilde{\boldsymbol{\sigma}} + \varepsilon + \boldsymbol{\Xi} \tag{25}$$

where $\widetilde{\mathbf{W}} = \mathbf{W} - \widehat{\mathbf{W}}$. Now the Taylor series is used for approximating $\widetilde{\boldsymbol{\sigma}}$ in Eq. (25), by which the dynamics of the filtered tracking error vector becomes:

$$\dot{\boldsymbol{\varphi}} = -\mathbf{K}\boldsymbol{\varphi} + \widetilde{\mathbf{W}}^{\mathbf{T}}(\widehat{\boldsymbol{\sigma}} - \acute{\boldsymbol{\sigma}}\widehat{\mathbf{V}}^{\mathbf{T}}\mathbf{x}) + \widehat{\mathbf{W}}^{\mathbf{T}}\acute{\boldsymbol{\sigma}}\widetilde{\mathbf{V}}^{\mathbf{T}}\mathbf{x} + \varepsilon + \boldsymbol{\Xi} + \boldsymbol{\delta} \tag{26}$$

where $\boldsymbol{\delta} = \widetilde{\mathbf{W}}^{\mathbf{T}}\acute{\boldsymbol{\sigma}}\widetilde{\mathbf{V}}^{\mathbf{T}}\mathbf{x} + \mathbf{W}^{\mathbf{T}}\mathbf{O}(\widetilde{\mathbf{V}}^{\mathbf{T}}\mathbf{x})$ is the disturbance due to the high-order terms in the Taylor series.

In this work, let us propose the online weight tuning algorithm for the NN weights as follows:

$$\dot{\widehat{\mathbf{W}}} = \mathbf{H_1}(\widehat{\boldsymbol{\sigma}}\boldsymbol{\varphi}^{\mathbf{T}} - \acute{\boldsymbol{\sigma}}\widehat{\mathbf{V}}^{\mathbf{T}}\mathbf{x}\boldsymbol{\varphi}^{\mathbf{T}} - \alpha||\boldsymbol{\varphi}||\widehat{\mathbf{W}}) \tag{27}$$

$$\dot{\widehat{\mathbf{V}}} = \mathbf{H_2}(\mathbf{x}\boldsymbol{\varphi}^{\mathbf{T}}\widehat{\mathbf{W}}^{\mathbf{T}}\acute{\boldsymbol{\sigma}} - \alpha||\boldsymbol{\varphi}||\widehat{\mathbf{V}}) \tag{28}$$

where $\mathbf{H_1}$ is an $(N_2+1)\times N_3$ positive definition constant matrix. $\mathbf{H_2}$ is an $(N_1+1)\times N_2$ positive definition constant matrix. α is positive constants. All of $\mathbf{H_1}$ $\mathbf{H_2}$, and α can be chosen arbitrarily. The first terms in the parentheses in Eqs. (27) and (28) show the standard backpropagation algorithm. The last terms in the parentheses express the $e-$modification [3] required for ensuring that the estimations of the weights are bounded.

3. The stability

Assumption 2 *It is assumed that* $\boldsymbol{\Xi}$ *and* $\boldsymbol{\delta}$ *in Eq. (26) are bounded. Particularly,* $\|\Xi\| \le \mathbf{b}_{\boldsymbol{\Xi}}$, $||\boldsymbol{\delta}|| \le \mathbf{b}_{\delta}$, *with* $\mathbf{b}_{\boldsymbol{\Xi}}$, $\mathbf{b}_{\delta}$ *being the upper bound of* $\boldsymbol{\Xi}$ *and* $\boldsymbol{\delta}$, *respectively.*

Assumption 3 *The linear velocity as well as the linear acceleration of the desired trajectory are bounded. To be specific, all of* $\dot{x}_D, \dot{y}_D, \ddot{x}_D$, *and* $\ddot{y}_D$ *in Eq. (13) are bounded.*

Definition 1 *For convenience, let us define matrices as follows:* $\mathbf{Z} = \mathbf{diag}\,\{\mathbf{W},\mathbf{V}\}$, $\widehat{\mathbf{Z}} = \mathbf{diag}\left\{\widehat{\mathbf{W}},\widehat{\mathbf{V}}\right\}$, $\widetilde{\mathbf{Z}} = \mathbf{diag}\left\{\widetilde{\mathbf{W}},\widetilde{\mathbf{V}}\right\}$. *Here, diag{ } illustrates a diagonal matrix.*

Assumption 4 *The ideal parameter* $\mathbf{Z}$ *is bounded by a known upper bound as* $\|\mathbf{Z}\|_{\mathbf{F}} \le Z_M$ *where* $\|\bullet\|_{\mathbf{F}}$ *is the Frobenius norm.*

It is worth noting that Z_M is only used with the purpose of analyzing stability.

Theorem 1 *For the WMR subject to wheel slip as in Eq. (11) and Figure 1, let the control input be given by Eq. (23) and the online weight tuning algorithm be provided by Eqs. (27) and (28). Then, according to Lyapunov theory and LaSalle extension, the stability of the closed-loop system is assured to achieve the desired tracking performance where the filtered tracking error vector* $\boldsymbol{\varphi}$ *as well as the vector of the weight errors* $\widetilde{\mathbf{Z}}$ *are uniformly ultimately bounded [3] and* $\boldsymbol{\varphi}$ *can be kept arbitrarily small.*

Proof Let us define a Lyapunov candidate function as follows:

$$L = \frac{1}{2}\boldsymbol{\varphi}^{\mathbf{T}}\boldsymbol{\varphi} + \frac{1}{2}tr(\widetilde{\mathbf{W}}^{\mathbf{T}}\mathbf{H_1^{-1}}\widetilde{\mathbf{W}}) + \frac{1}{2}tr(\widetilde{\mathbf{V}}^{\mathbf{T}}\mathbf{H_2^{-1}}\widetilde{\mathbf{V}}), \tag{29}$$

where tr(•) denotes the trace of the matrix.

Taking the first derivative with time and noting that $\dot{\widetilde{\mathbf{W}}} = -\dot{\widehat{\mathbf{W}}}$ and $\dot{\widetilde{\mathbf{V}}} = -\dot{\widehat{\mathbf{V}}}$ yields:

$$\dot{L} = \boldsymbol{\varphi}^{\mathbf{T}}\dot{\boldsymbol{\varphi}} - \mathrm{tr}(\widetilde{\mathbf{W}}^{\mathbf{T}}\mathbf{H_1^{-1}}\dot{\widehat{\mathbf{W}}}) - \mathrm{tr}(\widetilde{\mathbf{V}}^{\mathbf{T}}\mathbf{H_2^{-1}}\dot{\widehat{\mathbf{V}}}) \tag{30}$$

Substitution of Eq. (26) into Eq. (30) results in:

$$\dot{L} = \boldsymbol{\varphi}^{\mathbf{T}}[-\mathbf{K}\boldsymbol{\varphi} + \widetilde{\mathbf{W}}^{\mathbf{T}}(\widehat{\boldsymbol{\sigma}} - \acute{\boldsymbol{\sigma}}\widehat{\mathbf{V}}^{\mathbf{T}}\mathbf{x}) + \widehat{\mathbf{W}}^{\mathbf{T}}\acute{\boldsymbol{\sigma}}\widetilde{\mathbf{V}}^{\mathbf{T}}\mathbf{x} + \boldsymbol{\varepsilon} + \boldsymbol{\Xi} + \boldsymbol{\delta}] - \ \mathrm{tr}(\widetilde{\mathbf{W}}^{\mathbf{T}}\mathbf{H}_{\mathbf{1}}^{-\mathbf{1}}\dot{\widehat{\mathbf{W}}}) - \ \mathrm{tr}(\widetilde{\mathbf{V}}^{\mathbf{T}}\mathbf{H}_{\mathbf{2}}\dot{\widehat{\mathbf{V}}}), \quad (31)$$

Due to $\boldsymbol{\varphi}^{\mathbf{T}}\widetilde{\mathbf{W}}^{\mathbf{T}}\acute{\boldsymbol{\sigma}}\widehat{\mathbf{V}}^{\mathbf{T}}\mathbf{x} = \ \mathrm{tr}(\widetilde{\mathbf{W}}^{\mathbf{T}}\acute{\boldsymbol{\sigma}}\widehat{\mathbf{V}}^{\mathbf{T}}\mathbf{x}\boldsymbol{\varphi}^{\mathbf{T}}), \boldsymbol{\varphi}^{\mathbf{T}}\widehat{\mathbf{W}}^{\mathbf{T}}\acute{\boldsymbol{\sigma}}\widetilde{\mathbf{V}}^{\mathbf{T}}\mathbf{x} = \mathrm{tr}(\widetilde{\mathbf{V}}^{\mathbf{T}}\mathbf{x}\boldsymbol{\varphi}^{\mathbf{T}}\widehat{\mathbf{W}}^{\mathbf{T}}\acute{\boldsymbol{\sigma}})$ and $\boldsymbol{\varphi}^{\mathbf{T}}\widetilde{\mathbf{W}}^{\mathbf{T}}\widehat{\boldsymbol{\sigma}} = \ \mathrm{tr}(\widetilde{\mathbf{W}}^{\mathbf{T}}\widehat{\boldsymbol{\sigma}}\boldsymbol{\varphi}^{\mathbf{T}})$, (31) becomes

$$\dot{L} = \boldsymbol{\varphi}^{\mathbf{T}}[-\mathbf{K}\boldsymbol{\varphi} + \boldsymbol{\varepsilon} + \boldsymbol{\Xi} + \boldsymbol{\delta}] + \ \mathrm{tr}[\widetilde{\mathbf{W}}^{\mathbf{T}}(\mathbf{H}_{\mathbf{1}}^{-\mathbf{1}}\dot{\widehat{\mathbf{W}}} - \widehat{\boldsymbol{\sigma}}\boldsymbol{\varphi}^{\mathbf{T}} + \acute{\boldsymbol{\sigma}}\widehat{\mathbf{V}}^{\mathbf{T}}\mathbf{x}\boldsymbol{\varphi}^{\mathbf{T}})] - \mathrm{tr}[\widetilde{\mathbf{V}}^{\mathbf{T}}(\mathbf{H}_{\mathbf{2}}^{-\mathbf{1}}\dot{\widehat{\mathbf{V}}} - \mathbf{x}\boldsymbol{\varphi}^{\mathbf{T}}\widehat{\mathbf{W}}^{\mathbf{T}}\acute{\boldsymbol{\sigma}})] \quad (32)$$

Substituting Eqs. (27) and (28) into Eq. (32) leads to

$$\dot{L} = \boldsymbol{\varphi}^{\mathbf{T}}(-\mathbf{K}\boldsymbol{\varphi} + \boldsymbol{\varepsilon} + \boldsymbol{\Xi} + \boldsymbol{\delta}) + \alpha||\boldsymbol{\varphi}||(\widetilde{\mathbf{Z}}^{\mathbf{T}}\widehat{\mathbf{Z}}) \quad (33)$$

One can easily write $\widehat{\mathbf{Z}} = \mathbf{Z} - \widetilde{\mathbf{Z}}$. It is helpful to point out the following inequality:

$$\widehat{\mathbf{Z}}^{\mathbf{T}}(\mathbf{Z} - \widetilde{\mathbf{Z}}) \leq Z_M||\widetilde{\mathbf{Z}}||_F - ||\widetilde{\mathbf{Z}}||_F^{\mathbf{2}} \quad (34)$$

According to Assumptions 1, 2, 3, and 4 and Eq. (34), one achieves an inequality as follows:

$$\dot{L} \leq ||\boldsymbol{\varphi}||[-K_{min}||\boldsymbol{\varphi}|| + b_{\varepsilon} + b_{\boldsymbol{\Xi}} + b_{\delta} + \alpha(Z_M||\widetilde{\mathbf{Z}}||_F - ||\widetilde{\mathbf{Z}}||_F^2)] \quad (35)$$

where $K_{\min}$ is the minimum singular value of $\mathbf{K}$.

Because of the fact that $Z_M\left\|\widetilde{\mathbf{Z}}\right\|_F \leq \frac{1}{2}Z_M^2 + \frac{1}{2}\left\|\widetilde{\mathbf{Z}}\right\|_F^2$, one has the following inequality:

$$\dot{L} \leq ||\boldsymbol{\varphi}||[-K_{\min}||\boldsymbol{\varphi}|| - \frac{1}{2}\alpha||\widetilde{\mathbf{Z}}||_F^2 + b_{\varepsilon} + b_{\boldsymbol{\Xi}} + b_{\delta} + \frac{1}{2}\alpha Z_M^2] \quad (36)$$

Observing Eq. (36) reveals that $\dot{L}$ is guaranteed to be negative definite as long as the term in the parentheses is negative. Particularly, $\dot{L} < 0$ is assured if the following inequality is correct:

$$K_{\min}||\boldsymbol{\varphi}|| + \frac{1}{2}\alpha||\widetilde{\mathbf{Z}}||_F^2 > b_{\varepsilon} + b_{\boldsymbol{\Xi}} + b_{\delta} + \frac{1}{2}\alpha Z_M^2 \quad (37)$$

As a result, according to Lyapunov theory and LaSalle extension, $\boldsymbol{\varphi}$ as well as $\widetilde{\mathbf{Z}}$ are uniformly ultimately bounded in a compact set as follows:

$$\mathbf{U_B} = \left\{\boldsymbol{\varphi}, \widetilde{\mathbf{Z}} \middle| K_{\min}||\boldsymbol{\varphi}|| + \frac{1}{2}\alpha||\widetilde{\mathbf{Z}}||_F^2 \leq b_{\varepsilon} + b_{\boldsymbol{\Xi}} + b_{\delta} + \frac{1}{2}\alpha Z_M^2\right\} \quad (38)$$

Furthermore, it is worth noting that $\boldsymbol{\varphi}$ can be made arbitrarily small by choosing the gains $\mathbf{K}$ suitably. To be specific, the bigger $\mathbf{K}$ is, the smaller $\boldsymbol{\varphi}$ and is. □

4. Simulation results

To show the validity of the proposed control law, we implemented computer simulations for trajectory tracking of the WMR with the parameters shown in the Table. We compared the tracking performance of the proposed control method with that of the feedback linearization control method [8] with the purpose of validating the advantages of the proposed control method.

For comparison, both of two these methods mentioned above were performed under a condition in which there existed model uncertainties and unknown bounded disturbances (in other words, $\boldsymbol{\tau}_{\mathbf{d}} \neq \mathbf{0}$), and moreover the velocities and accelerations of the wheel slips were not measured. Without loss of generality, it was assumed that $\boldsymbol{\tau}_{\mathbf{d}} = [3 + \sin(0.5t), 2.5 + \cos 0.4t]^T$, $\widehat{\mathbf{M}} = 0.7\mathbf{M}$, and the velocities of the unknown wheel slips were given by $[\dot{\gamma}_R, \dot{\gamma}_L, \dot{\eta}]^T = [2\sin t, 1.5\cos 0.5t, 0.5]^T$ (m/s) for all $t > 2$ (s). The initial posture in the world coordinate system O-XY is $x_P = C = 0.5$ (m), $y_P = 0$ (m), and $\theta = 0.1$ (rad).

The control parameters were chosen as $\mathbf{K} = \mathbf{diag}([6,\ 6])$, $\boldsymbol{\Lambda} = \mathbf{diag}\ ([2,\ 2])$. The hidden layer had 10 neurons. The weight tuning gains were set as $\mathbf{H_1} = \mathbf{diag(10)}_{\mathbf{11\times 2}}$, $\mathbf{H_2} = \mathbf{diag(10)}_{\mathbf{5\times 10}}$, and $\alpha = 0.5$ The initial conditions of the weight matrices were chosen as random numbers in [0, 1] as $\widehat{W}_{\mathbf{0}} = [\mathbf{rand(0,1)}]_{\mathbf{11\times 2}}$, $\widehat{V}_{\mathbf{0}} = [\mathbf{rand(0,1)}]_{\mathbf{5\times 10}}$.

For illustration, the two following examples were implemented in MATLAB/Simulink software.

Example 1 *Target D moved on a straight line with the motion equation described as follows:*

$$\begin{cases} x_D = 3 + 0.75t \\ y_D = -2 + 0.5t \end{cases} \tag{39}$$

Obviously, in Figures 4 and 5, we can easily see that when the accelerations and velocities of the unknown wheel slips were not measured and model uncertainties and unknown bounded disturbances existed, the control approach in [8] could not compensate the undesired effects while the proposed control method effectively dealt with the undesired effects.

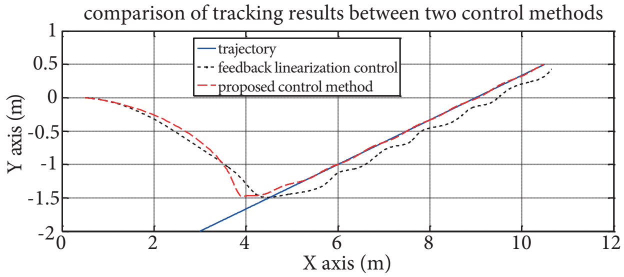

Figure 4. Comparison of the trajectories in Example 1.

In addition, as can be seen in Figure 6, the control inputs and some of the weights have been bounded.

Example 2 *Target D moved on a circular path with the motion equation described as follows:*

$$\begin{cases} x_D = 5 - 3\cos 0.25t \\ y_D = 2 + 3\sin 0.25t \end{cases} \tag{40}$$

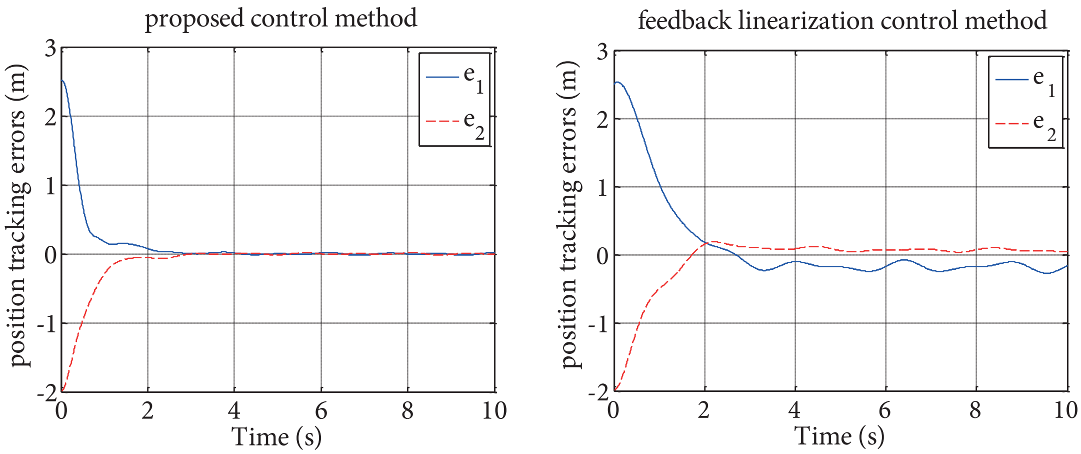

Figure 5. Comparison of tracking errors in Example 1.

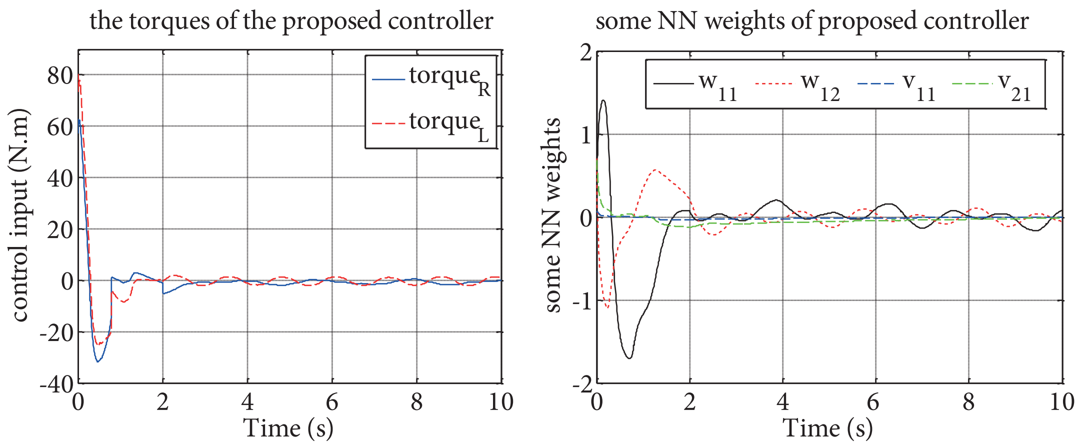

Figure 6. Torques and some weights of proposed control method in Example 1.

It is interesting when looking at Figures 7 and 8. Regardless of the unknown wheel slips, model uncertainties, and unknown bounded disturbances, the proposed control method managed to compensate the harmful effects very effectively, while the control approach in [8] could not.

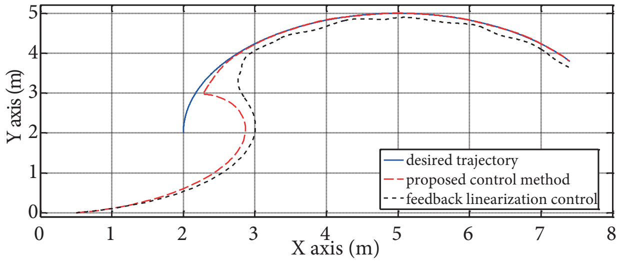

Figure 7. Comparison of tracking results in Example 2.

It should be noted that the position tracking errors of the proposed control method almost converged to zero, as shown in Figures 5 and 8, whereas that of the feedback linearization control method [8] did not. As a consequence, the tracking performance of the former is better than that of the latter.

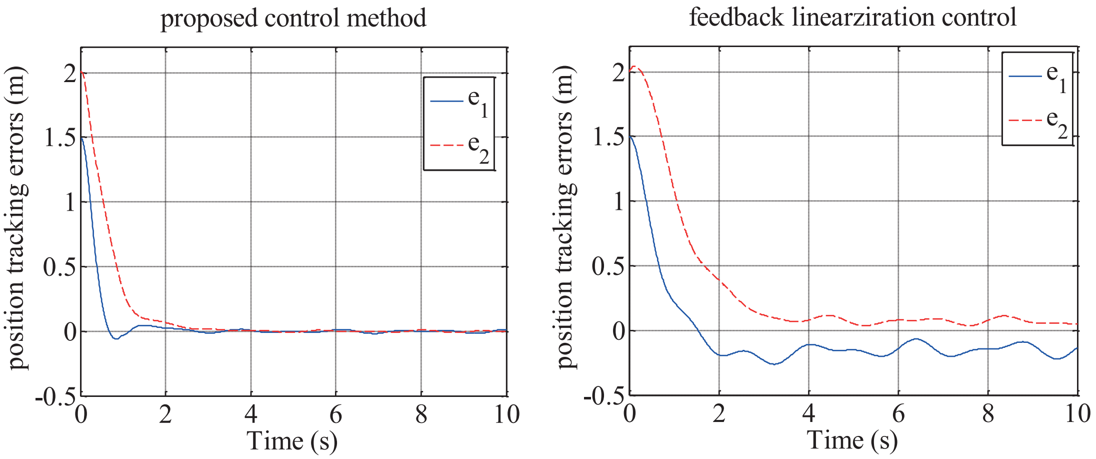

Figure 8. Comparison of tracking errors in Example 2.

It is apparent that due to the convergence of φ to an adjustable small neighborhood of the origin, the position tracking error vector, **e**, in Eq. (14) converged to a small neighborhood of the origin. Hence, $\boldsymbol{\zeta_1}$ converged to a small neighborhood of C. Therefore, according to Remark 2, one can easily conclude that **h** in Eq. (13) is invertible.

In addition, the control inputs and some the weights in this example were bounded, as shown in Figure 9.

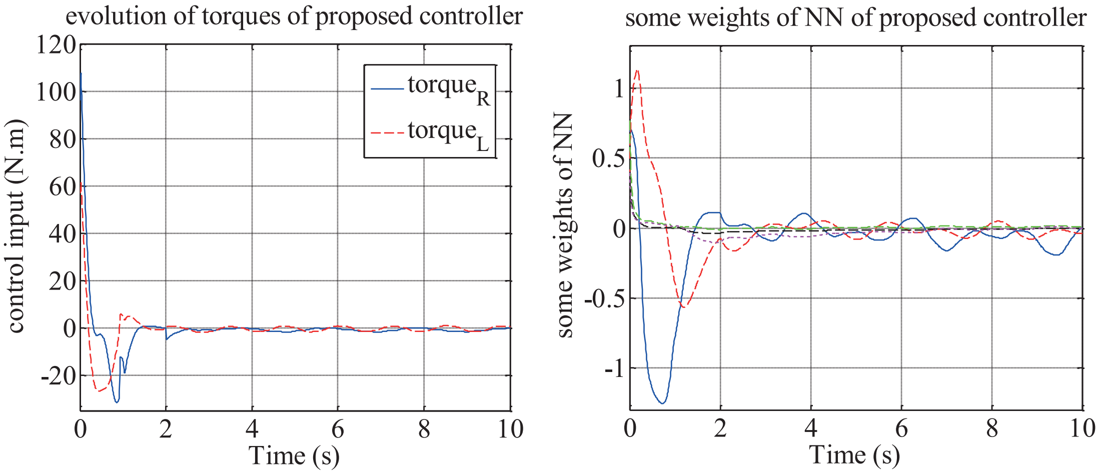

Figure 9. Torques and some weights of the proposed control method in Example 2.

From these simulation results, one can easily conclude that the proposed control method is correct and effective.

Remark 5 *For comparison purposes, the feedback linearization control method proposed in [8] was simulated with a more realistic condition: besides ignoring the measurements for the accelerations and velocities of the wheel slips, there also existed both external disturbances and model uncertainties (in [8] performed under an ideal and unrealistic condition where in addition to measuring the accelerations and velocities of the wheel slips exactly, there existed no external disturbances or model uncertainties). Similar conditions were used for our proposed method for the convenience of comparison.*

5. Discussion

In comparison with the work given in [5], we illustrate the differences as follows:

- In this work, we have proposed one adaptive tracking controller based on the sliding mode control technique with only one control closed loop, whereas the work in [5] utilized backstepping techniques (backstepping from kinematics into dynamics) with two control closed loops where the outer one is the kinematic control closed loop and the inner one is the dynamic control closed loop.
- Furthermore, the work in [5] only dealt with longitudinal slips of each driving wheel, but the lateral slip was not considered, while our proposed controller has managed to compensate both longitudinal and lateral slips.
- In addition, the work in [5] employed slip ratios that heavily depended on a gyro-sensor and odometry for designing the kinematic control law, whereas our work did not.

In comparison with the work given in [10], the work in [10] proposed a model-based control method using an accurate traction model, where the adhesion coefficient between the wheels and the hard flat surface is a function of the wheel slips for improving tracking performance of a WMR, whereas our proposed control method has not.

In comparison with the work in [11], we show the differences as follows:

- While the work in [11] built the online adaptive weight updating laws by making an objective function minimal by using the gradients of this objective function, we, in this proposed control method, have built an online adaptive tuning algorithm for the neural network weights from the Lyapunov stability analysis.
- Besides, the work of [11] addressed the position tracking control problem in the world (global) Cartesian coordinate system (O-XY), but our work has addressed this problem in the body Cartesian coordinate system, M-XY, attached to the platform of the mobile robot.

Additionally, another difference between our proposed control method and other methods, except for the one in [8], is that our proposed control method must check the invertible property of matrix **h** in Eq. (13) as in Remark 2 before designing the control law, and then the control law must always check and guarantee that matrix **h** is invertible in the implementation of the closed-loop control system.

In conclusion, in this work, an adaptive tracking controller based on a three-layer NN with the online weight tuning algorithm was developed to allow the WMR to track a desired trajectory with the desired tracking performance. It has been shown that the convergence of the position tracking errors to an arbitrarily small neighborhood of the origin was guaranteed by the standard Lyapunov theory and LaSalle extension. The results of the computer simulations confirmed the validity and advantages of the proposed control method.

Acknowledgment

This work was supported by the Vietnam Academy of Science and Technology, Grant No: VAST01.06/17-18.

References

[1] Becerra H, Nicolas G, Sagues C. A sliding-mode-control law for mobile robots based on epipolar visual servoing from three views. IEEE T Robot 2011; 27: 175-183.

[2] Park B, Yoo S, Choi Y, Park J. A simple adaptive control approach for trajectory tracking of nonholonomic electrically driven mobile robots. IEEE T Contr Syst T 2010; 18: 1199-1206.

[3] Fierro R, Lewis F. Control of a nonholonomic mobile robot using neural networks. IEEE T Neural Networ 1998; 9: 589-600.

[4] Lee T, Song K, Lee C, Teng C. Tracking control of unicycle-modeled mobile robots using a saturation feedback controller. IEEE T Contr Syst T 2001; 9: 305-318.

[5] Gao H, Song X, Ding L, Xia K, Li N, Deng Z. Adaptive motion control of wheeled mobile robot with unknown slippage. Int J Contr 2014; 87: 1513-1522.

[6] Seyr M, Jakubek S. Proprioceptive navigation, slip estimation and slip control for autonomous wheeled mobile robots. In: IEEE 2006 Conference on Robotics, Automation and Mechatronics; 7–9 June 2006; Bangkok, Thailand. New York, NY, USA: IEEE. pp. 1-6.

[7] Boon LC, Danwei W. Integrated estimation for wheeled mobile robot posture, velocities, and wheel skidding perturbations. In: IEEE 2007 International Conference on Robotics and Automation; 10–14 April 2007; Rome, Italy. New York, NY, USA: IEEE. pp. 2355-2360.

[8] Tinh NV, Linh NT, Cat PT, Tuan PM, Anh MN, Anh NP. Modeling and feedback linearization control of a nonholonomic wheeled mobile robot with longitudinal, lateral slips. In: IEEE 2016 International Conference on Automation Science and Engineering; 21–24 August 2016; Fort Worth, TX, USA. New York, NY, USA: IEEE. pp. 996-1001.

[9] Wang D, Low C. Modeling and analysis of skidding and slipping in wheeled mobile robots: control design perspective. IEEE T Robot 2008; 24: 676-687.

[10] Balakrishna R, Ghosal A. Modeling of slip for wheeled mobile robots. IEEE T Robotic Autom 1995; 11: 126-132.

[11] Bach H, Kang H. Neural network-based adaptive tracking control of mobile robots in the presence of wheel slip and external disturbance force. Neurocomputing 2016; 188: 12-22.